

Article

Jets Studies in Central and Forward Regions at Current and Expected Large Hadron Collider Future Energies

M. A. Mahmoud ^{1,2,*} , Somaia Hamdi ^{2,3}, A. Radi ^{4,5} , M. A. El-Borie ³ and E. A. Tayel ^{2,3}

¹ Physics Department, Faculty of Science, Fayoum University, El-Fayoum 63514, Egypt
² Center for High Energy Physics (CHEP-FU), Fayoum University, El-Fayoum 63514, Egypt
³ Physics Department, Faculty of Science, Alexandria University, Alexandria 21526, Egypt
⁴ Department of Physics, College of Science, Sultan Qaboos University, Muscat 123, Oman
⁵ Department of Physics, College of Science, Ain Sham University, Cairo 11566, Egypt
* Correspondence: mohammed.attia@cern.ch

Abstract: The present work presents a study of jet production in the central region ($|\eta| < 2.5$) and the forward region ($3 < |\eta| < 5$) in proton–proton collisions at different energies: $\sqrt{s} = 13.6$ TeV, $\sqrt{s} = 20$ TeV, and $\sqrt{s} = 27$ TeV. These energies are the present and expected future energies of the Large Hadron Collider. In addition, the measurement of dijets—where the dijet selected is the one leading the jet in the central region and the second jet is the one with the sub-leading role in the forward region—was investigated with the same collision energies. Jets are reconstructed with the anti-kT ($R = 0.5$) algorithm in the transverse momentum range $p_T = 15$ –1000 GeV/c. Different Monte Carlo event generators were used: PYTHIA, HERWIG, and EPOS-LHC. The momentum, multiplicity, energy, pseudorapidity, and azimuthal angle of the jets were measured. In addition, the dijet multiplicity and the difference in the azimuthal angle were measured. The generation of events was carried out using the Rivet analysis framework. It is observed that, when the energy of the collision increases, the production of the jets in the central and forward regions and the dijets multiplicity increase; overall an agreement is observed between the three event generators. The disagreement between the different generators points to potential areas for development or additional study.

Keywords: LHC; central jets; forward jets; dijets; future energies; PYTHIA; HERWIG; EPOS-LHC



Citation: Mahmoud, M.A.; Hamdi, S.; Radi, A.; El-Borie, M.A.; Tayel, E.A. Jets Studies in Central and Forward Regions at Current and Expected Large Hadron Collider Future Energies. *Universe* **2024**, *10*, 154. <https://doi.org/10.3390/universe10040154>

Academic Editor: Sevil Salur

Received: 4 January 2024

Revised: 1 March 2024

Accepted: 13 March 2024

Published: 25 March 2024



Copyright: © 2024 by the authors. Licensee MDPI, Basel, Switzerland. This article is an open access article distributed under the terms and conditions of the Creative Commons Attribution (CC BY) license (<https://creativecommons.org/licenses/by/4.0/>).

1. Introduction

Strong interactions are described by quantum chromodynamics (QCD), the study of the interactions between quarks and gluons. These quarks and gluons are called partons and are not observed independently outside of hadrons because of quark confinement. These partons are confined to form hadrons, which are detected by the detector [1]. The process of creating hadrons is known as “hadronization”, and it leads to the production of particles known as “jets” [2]. Thus, jets are collimated sprays of hadrons created in large quantities during proton–proton (pp) collisions in the Large Hadron Collider (LHC). These jets appear as cones with a radius of R and are driven in the same direction [3].

The jet is one of the most common phenomena in pp collisions at the LHC. It is produced when the hard-scattering process initiates a jet-like cascade of particles [4]. Heavy particles like top quarks, W , Z , and Higgs bosons that decay hadronically can produce jets. So, the source of particles can be identified from the properties of the reconstructed jets [5]. Searches for new particles and studying physics beyond the standard model can be significantly improved with the help of such particle-identifying information, which gives excellent insights into collision events and helps in differentiating events originating from different physics processes [6]. The jet size or radius R is localized around the highest concentration of energy in the event and provides the distance in the rapidity azimuthal plane ($\eta - \phi$). Jet size is used to determine whether the particle belongs to the jets or not, i.e., above a specific R value, the hadron no longer belongs to the jet [7].

There are different types of jets: jets with a distance parameter $R = 0.4$ (small-R jets) and jets with $R = 1.0$ (large-R jets). Small-R jets are produced from light particles like quarks and gluons [8]; meanwhile, large-R jets are produced from massive particles like W and Z bosons, top quarks, and the Higgs bosons [9].

The central jets play a major role in energy calibration, background estimation, and fundamental interactions and precision measurements in high-energy collisions. Forward jets are essential in several areas of high-energy physics study, including the understanding of QCD through vector-jet modeling and Higgs production mechanisms. Jet formation in hadron collisions is affected by underlying partonic processes as well as initial-state and final-state radiation (ISR and FSR) [10]. Measurements of jet cross-sections at earlier colliders are explained well by perturbative calculations over several orders of magnitude. For jets in central pseudorapidity regions (central jets within $|\eta| < 2.4$), where the momentum fraction of the incoming partons (x_1, x_2) were of the same order, those with pseudorapidity $3.2 < |\eta| < 5$ (i.e., forward or backward jets) are a result of interactions between colliding partons and differing momentum fractions, where ($x_1 \ll x_2$) [11]. Jet definition or jet algorithms refer to the process or method of reconstructing the jets from a collection of parameters and hadrons in the final state of the collision. Many jet algorithms have been proposed; however, the two primary groups are the cone and sequential recombination methods [12].

The cone algorithm is based on the idea that jets represent the event’s energy flow. So, it is independent of the merging process and is based on the concept of a stable cone, which means that, in the rapidity–azimuthal angle plane, the 4-momentum of all particles within a set radius R around the cone center can be added [13]. If the summation of the 4-momentum of the particles is in the direction of the center of the cone, then the cone is considered to be a stable cone. If the sum of 4-momentum is above a certain threshold value, then the particle is considered a jet. There are different types of cone algorithms, and none of them are infrared or collinear-safe except for the SIS cone [14].

The premise of sequential recombination algorithms is that jets are considered to be partons (quarks and gluons). These algorithms try to recombine two particles into one [15]. The various recombination algorithms utilized in hadronic collisions belong to the generalized- kt algorithm, which builds a cluster by making a comparison between variables d_{ij} and d_{iB} ; here, d_{ij} is defined as the distance between two particles or clustered pseudojets i and j , and d_{iB} is defined as the distance between i and the beam [16]. First, the particles produced in the event should be listed; then, the distances of d_{ij} and d_{iB} should be measured, where the distance between all pairs of partons and the beam distance are defined, as shown in [17]:

$$d_{ij} = \frac{\min(k_{t,i}^{2p}, k_{t,j}^{2p}) \Delta_{ij}^2}{R^2}$$

and

$$d_{iB} = k_{t,i}^{2p}$$

To determine the smallest distance of them, if d_{ij} is the smallest, then i and j are replaced with a single new particle whose momentum is $p_i + p_j$. This particle is called a pseudojet. The algorithm continues to compare between i and other neighboring particles. If the smallest distance is d_{iB} , then parton i has been erased from the list of the particles, which is declared as a jet. Repeat this process until no objects are left to compare [18]. Jet measurements at the LHC are nearly invariably reconstructed using the anti- kt methodology. The anti- kt algorithm is the third type of the generalized- kt algorithm, where $p = -1$. The anti- kt algorithm is a collinear–infrared safety algorithm and it does not lead to irregular jet shapes [19]. For collinear safety, $\Delta R = 0$, which means that the partons i and j are radiated in the same direction; then, $d_{ij} \approx 0$, i.e., “it is the smallest distance”; so, we merge the partons i and j into a jet and remove them from the list. This means that one is safe from splitting up a bundle of particles into two different jets [20]. For infrared safety, $k_{t,i} \approx 0$; then, $d_{iB} = 0$; so, it is the smallest distance and thus we consider parton i as a jet [21].

Jet measurements in the hadron collider help in the search for new physics. These helped in the search for the standard model (SM) Higgs boson and the opened up the possibility of the existence of physics beyond the standard model [22]. The search for dark matter (DM) is based on searches for missing transverse energy produced with jets at the hadron collider. The missing transverse energy is an indicator for DM production [23]. Studying jets also helps in the search for the production of charginos and neutralinos in pp collision [24].

In the present manuscript, we make comparisons between the jets produced in the central regions ($|\eta| < 2.5$) and the forward regions ($3.2 < |\eta| < 5$) from pp collisions; these are reconstructed using the anti-kt algorithm, with a jet size ($R = 0.5$) at energies 13.6, 20, and 27 TeV, with transverse momentum range of 15–1000 GeV/c; also, dijets production was studied between the leading jet in the central region and the second jet which is sub-leading in the forward region, at the same energies. This study consists of five sections. The next section gives an introduction to some events generators which are used in the present study: PYTHIA, HERWIG, and EPOS-LHC. The third section discusses event selections, and the fourth section discusses the results and discussion. Finally, conclusions are discussed in the last section.

2. Monte Carlo Event Generators

Monte Carlo (MC) methods are also known as Monte Carlo simulations, initiated in the 1940s by John Von Neumann, Stanislaw Ulman, Enrico Fermi, and Nicholas Metropolis [25]. MC is a mathematical tool that is used to estimate the possible output of uncertain events and it is also used in particle physics to simulate a random number of events and then compare the simulated data to the real data [26]. MC event generators are used by experimenting researchers who use them for analysis; they are also used by theorists in making predictions for collider experiments and developing methods which they can suggest to experimenting researchers [27]. MC event generators are very important in high-energy collisions. There are many event generators used in particle physics, like EPOS-LHC [28], PYTHIA [29], HERWIG [30], MadGraph5 [31], and Sherpa [32].

2.1. PYTHIA Event Generator

PYTHIA is one of the most well-known general-purpose event generators [33]. It is based on the Lund string hadronization model [34]. It is a tool that can be used to generate events in high-energy collisions and includes a hard process library, models for initial-state radiation (ISR), final-state radiation (FSR), multiple parton interactions (MPIs), and particle decays [35]. It is also used to identify physics by comparing it to current data and to predict future physics. PYTHIA was originally created in FORTRAN; however, the code has now been remade in C++. PYTHIA is a LO MC event generator. PYTHIA now models hadron–hadron collisions, lepton–lepton collisions, gamma–hadron interactions, BSM particle decays, and dark matter annihilation into standard model particles [29]. PYTHIA may be used to solve a wide range of phenomenological problems related to particle physics, as well as those in astroparticle, nuclear, and neutrino physics [34].

Brief Description of the Lund String Model

The Lund string model is a mathematical framework in which strongly interacting particles known as hadrons are mathematically viewed as massless strings with ends that move at the speed of light in multidimensional space [36]. The color flux stretched between the initial $q\bar{q}$ is represented by a dynamical relativistic string in this model. The string breaks up into hadrons via $q\bar{q}$ pair production in its intense color field. Partons are created when two protons collide at the LHC. The string model is then used to stretch the string as the quarks move further apart, forming hadrons. The Lund string model is the basis of

PYTHIA event generator. In the Lund string model, the probability, P , for the production of a state of n mesons with momenta p_i ($i = 1, \dots, n$) is [37]:

$$P \propto \left\{ \prod_{i=1}^n [Nd^2 p_i \delta(p_i^2 - m^2)] \delta^{(2)}(\sum p_i - P_{tot}) \right\} \exp(-bA)$$

and the probability distribution function is given by [37]

$$f(z) = N \frac{(1-z)^a}{z} \exp\left(-\frac{bm^2}{z}\right)$$

2.2. HERWIG Event Generator

HERWIG is a general-purpose event generator for simulating high-energy lepton–lepton and hadron–hadron collisions, with a focus on precise QCD radiation modeling. It was originally written in FORTRAN and has since been rewritten in C++ [30]. As a result, it has many more advanced features than the previous version of FORTRAN. HERWIG is LO MC event generator. HERWIG simulates high-energy collisions in detail and includes the QCD jet generation in initial and final states and simulates hadron decays using matrix element description of the decay product distributions and spin correlations between individual decays [30]. HERWIG covers the suppression of QCD radiation from large particles in detail. In HERWIG, the underlying event is described by a model called multiple partonic scattering. HERWIG provides a cluster model of jet hadronization based on non-perturbative gluon splitting [38].

Brief Description of the Cluster Hadronization Model of HERWIG

The cluster model depends on the pre-confinement effect. In this model, at the end of the parton shower, all gluons have to split into quark–antiquark pairs. In the cluster model, the gluons are considered to be seeds instead of kinks in the string model. A new set of low-mass-color single quark–antiquark clusters is obtained after the splitting. These clusters undergo sequential cluster breakups along an axis that is defined by the constituent partons of the original cluster till all clusters fall below the cutoff value if their energy is higher than the cutoff value [39]. The cluster model of the hadronization of jets is based on non-perturbative gluon splitting; it is an intricate model of tau and hadron decays that includes a thorough treatment of spin correlations and off-shell effects. Matrix elements are used to provide the momenta of the decay products for numerous modes [40]. The weight for the production of the hadrons $a(q_1, \bar{q})$ and $b(q, \bar{q}_2)$ is given by:

$$W(a_{(q_1, \bar{q})}, b_{(q, \bar{q}_2)}) = P_q W_a w_b s_a s_b p^*_{a,b}$$

where P_q is the weight for the production of the quark–antiquark pairs; w_a and w_b are the weights for the production of individual hadrons; s_a and s_b are the suppression factors for the hadrons; $p^*_{a,b}$ is the momentum of the hadrons in the rest frame of the decaying cluster [40].

2.3. EPOS-LHC Event Generator

EPOS-LHC is a Monte Carlo hadronic generator with a minimal bias that is utilized for heavy ion interactions and aspires to simulate a wide range of LHC observable features, such as jets [41]. EPOS-LHC is a consistent quantum-mechanical multiple-scattering approach based on partons and strings; here, cross-sections and particle production are calculated consistently while accounting for energy conservation in both cases, in contrast to other models that do not account for energy conservation in cross-section calculations [42]. It is the only the hadronic model that consistently treats cross-section calculations and particle generation under energy conservation and it depends on the Gribov–Regge theory [43].

Brief Description of Hadronization Model of EPOS-LHC

Nucleus–nucleus scattering, including pp scattering, is the result of multiple elementary collisions occurring simultaneously. A basic scattering of this sort is known as the “parton ladder” [44]. Parton evolution from the projectile and target side towards the center are represented by a parton ladder. In the most basic scenario, the Dokshitzer–Gribov–Lipatov–Altarelli–Parisi (DGLAP) approach states that the evolution is controlled by an evolution Equation [45]. To differentiate between these partons and spectator partons, which will be covered later, we shall refer to these partons as ladder partons in this study. A while ago, it was discovered that a parton ladder of this kind could be considered to be a quasi-longitudinal color field which is easily handled like a relativistic string. In the language of relativistic strings, the intermediate gluons are treated as kink singularities, giving rise to a transversely moving part of the object. By generating quark–antiquark pairs, this flux tube decays, resulting in fragments that are recognized by their hadrons [46].

The initial conditions of hadronization in EPOS-LHC depend on strings, not on partons. The concept of initial conditions indicates the state of the system immediately before parton or hadron rescattering, such as in heavy ion (HI) collisions (final-state interactions), and after the initial- and final-state radiation of the jets when partons hadronize in high-energy physics (HEP) models [47].

3. Event Selections

PYTHIA, HERWIG, and EPOS-LHC were used to generate pp collisions at energies $\sqrt{s} = 13.6$ TeV, $\sqrt{s} = 20$ TeV, and $\sqrt{s} = 27$ TeV. These energies are the current and expected future energies of the Large Hadron Collider (LHC). The jets produced from pp collisions are selected according to the following criteria: the jet is produced in the central regions, according to the pseudorapidity region ($|\eta| < 2.5$), and in the forward regions, according to the pseudorapidity region ($3.2 < |\eta| < 5$), from pp collisions; these are reconstructed using the anti-kt algorithm, with jet size ($R = 0.5$) at energies of 13.6, 20, and 27 TeV; there are jet transverse momentum ranges of 15–1000 GeV/c using PYTHIA 8308, HERWIG 7.3, and EPOS-LHC event generators. The generation MC approaches using PYTHIA, HERWIG, and EPOS-LHC were carried out by applying the appropriate Rivet analysis framework [48] for the present study.

4. Results and Discussion

4.1. Jets Measurements

The jets p_T spectra in the central and forward regions with the minimum jet $p_T > 15$ GeV/c were produced from the pp collisions at an energy of $\sqrt{s} = 13.6$ TeV using different Monte Carlo simulation models: the PYTHIA, HERWIG, and EPOS-LHC event generators. The jets p_T spectra are presented in Figure 1. In the central region, the spectra start with an agreement between the three event generators; then, the data show a difference between the event generators. An agreement between HERWIG and EPOS-LHC is shown in some points, but an agreement between PYTHIA and HERWIG is shown in others. The spectra in the forward regions start with an agreement between PYTHIA and EPOS-LHC and then with an agreement between HERWIG and EPOS-LHC; then, they continue with a slight disagreement between the three event generators. EPOS-LHC has more data up to ≈ 220 GeV/c; the reason for this could be that every event generator has a unique set of underlying physics models and assumptions, as well as variations in how the parton showers and fragmentation processes are handled.

Figure 2 shows the p_T of the produced jets in the central and forward regions from the pp collisions at a higher energy $\sqrt{s} = 20$ TeV, produced using different event generators: PYTHIA, EPOS-LHC, and HERWIG. There was a minimum jet of $p_T > 15$ GeV/c. In the central region, an agreement between the three event generators is shown at the beginning of the spectrum; then, the spectra continue with a disagreement between the event generators. Furthermore, HERWIG presents more data than PYTHIA and EPOS-LHC, up to ≈ 450 GeV/c; this happened because HERWIG provides data that reveal unique

peculiarities at high p_T . These characteristics could be related to the underlying dynamics of parton interactions and hadronization. In the forward region, the spectra start with an agreement between the PYTHIA and EPOS-LHC event generators, which is similar to the spectrum at $\sqrt{s} = 13.6$ TeV. Then, they fall, with a bit of disagreement between the HERWIG and EPOS-LHC event generators; from ≈ 110 GeV/c to 140 GeV/c, a little disagreement between PYTHIA and HERWIG appears.

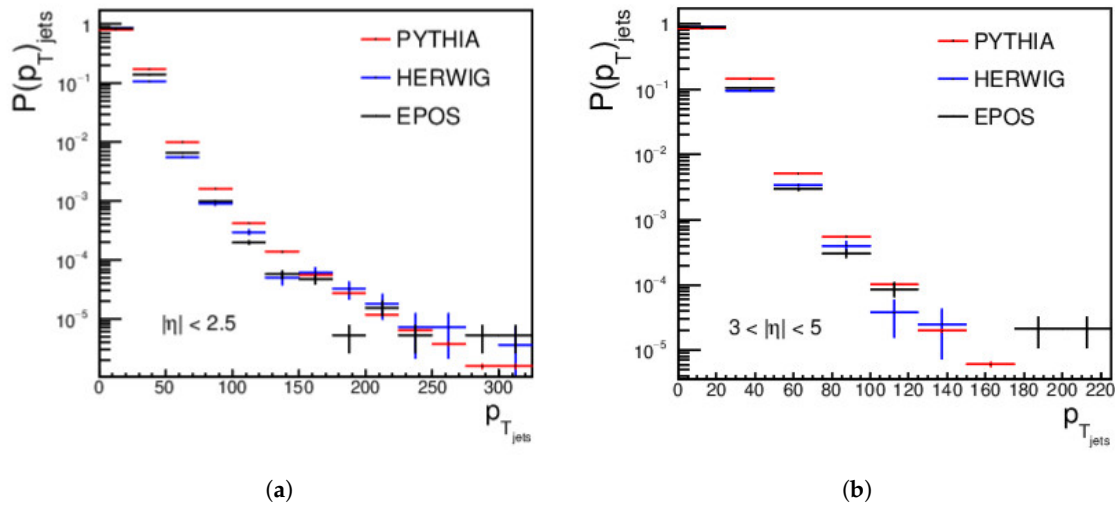


Figure 1. (a) MC comparison of central jet p_T (GeV/c) at $\sqrt{s} = 13.6$ TeV; (b) MC comparison of forward jet p_T (GeV/c) at $\sqrt{s} = 13.6$ TeV.

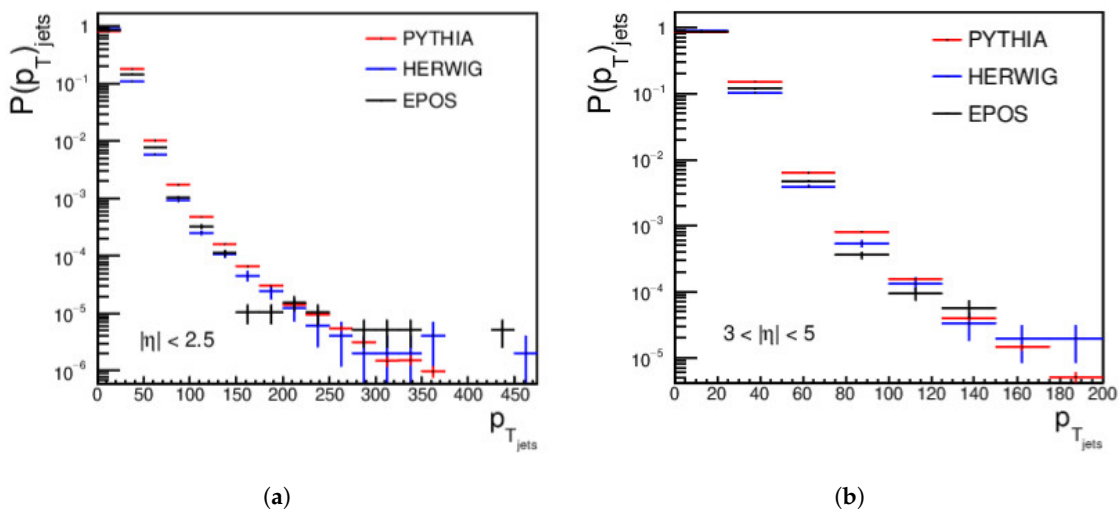


Figure 2. (a) MC comparison of central jet p_T (GeV/c) at $\sqrt{s} = 20$ TeV; (b) MC comparison of forward jet p_T (GeV/c) at $\sqrt{s} = 20$ TeV.

Finally, the p_T distributions for the central and forward jets, produced from pp collisions using PYTHIA, HERWIG, and EPOS-LHC at an energy of $\sqrt{s} = 27$ TeV and with a minimum jet of $p_T > 15$ GeV/c, are shown in Figure 3. For the central regions, a complete disagreement is shown between the three event generators. In the forward region, PYTHIA does not agree with HERWIG or EPOS-LHC, but a good agreement appears between HERWIG and EPOS-LHC from approximately 40 GeV/c to around 110 GeV/c; then, a disagreement between the three event generators occurs, as shown in Figure 3.

The multiplicity of jets in the forward and central regions is shown in Figure 4, with a minimum jet of $p_T > 15$ GeV/c produced by pp collisions at $\sqrt{s} = 13.6$ TeV using different Monte Carlo simulation models: PYTHIA, HERWIG, and EPOS-LHC. The jets' multiplicity

for the forward and central regions has no agreement between HERWIG and the other event generators. There is an agreement at the peak between PYTHIA and EPOS-LHC; then, the data show a slight difference between them. As shown in the figure, the jet multiplicity in the central region is larger than in the forward regions; the explanation for this is that, while the forward region encounters fewer parton collisions—and, hence, fewer jets—the central region exhibits stronger jet generation because of the intensive parton interactions and the efficient energy transfer.

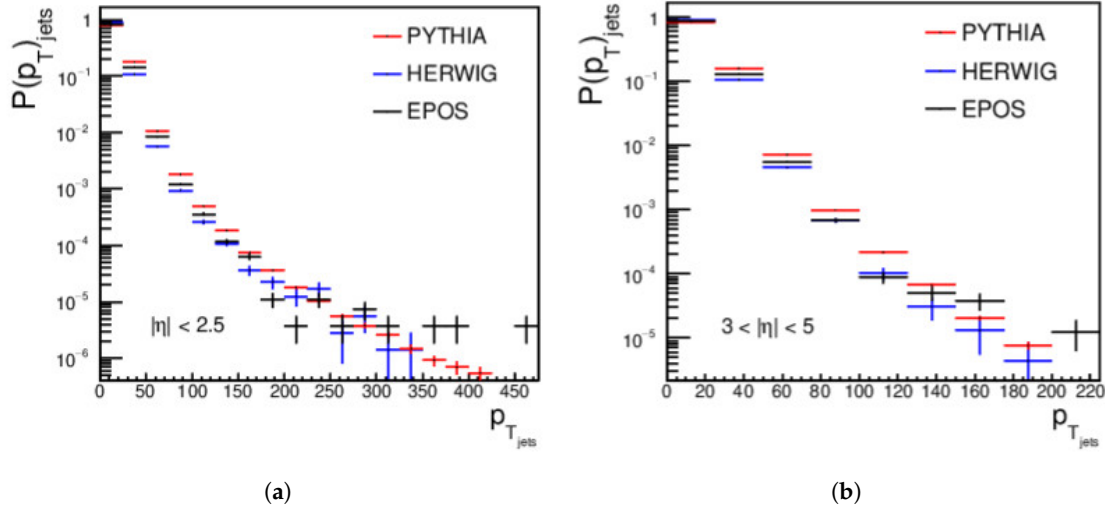


Figure 3. (a) MC comparison of central jet p_T (GeV/c) at $\sqrt{s} = 27$ TeV; (b) MC comparison of forward jet p_T (GeV/c) at $\sqrt{s} = 27$ TeV.

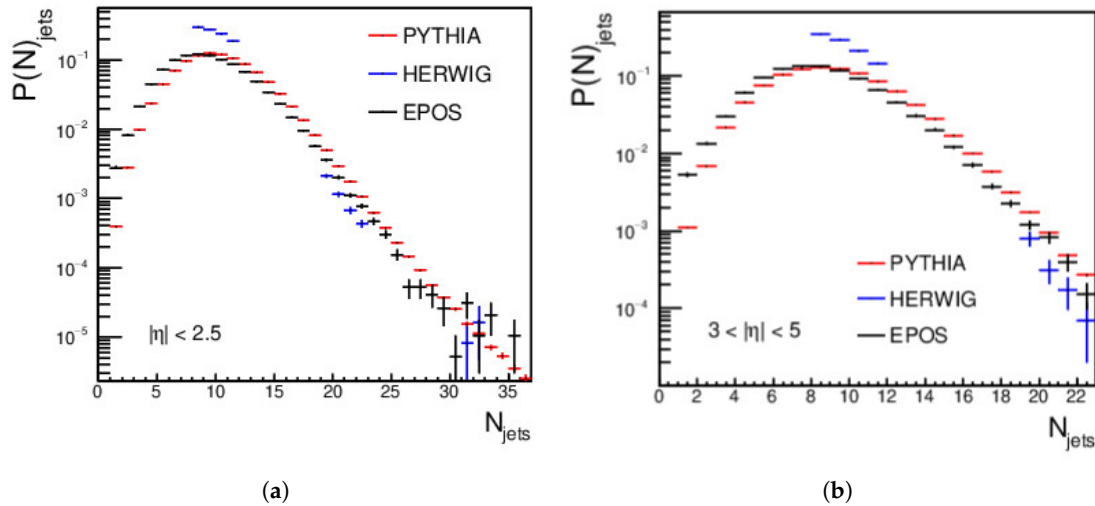


Figure 4. (a) MC comparison of jet multiplicity in the central regions at $\sqrt{s} = 13.6$ TeV; (b) MC comparison of jet multiplicity in the forward regions at $\sqrt{s} = 13.6$ TeV.

The jet multiplicity produced from the pp collisions at $\sqrt{s} = 20$ TeV in the central and forward regions with a minimum jet of $p_T > 15$ GeV/c is presented in Figure 5. For the forward and central regions, the jet multiplicity spectrum presents no agreement between HERWIG and the other event generators. The data show that there is a slight difference between PYTHIA and EPOS-LHC, except at the peak. It is clear that the jet multiplicity in the central regions is larger than the jet multiplicity in the forward regions. As shown in Figure 5, there is a similarity in the distribution of the jet multiplicity with the energy of collisions $\sqrt{s} = 13.6$ TeV; however, the jet multiplicity increases as the energy of pp collision increases.

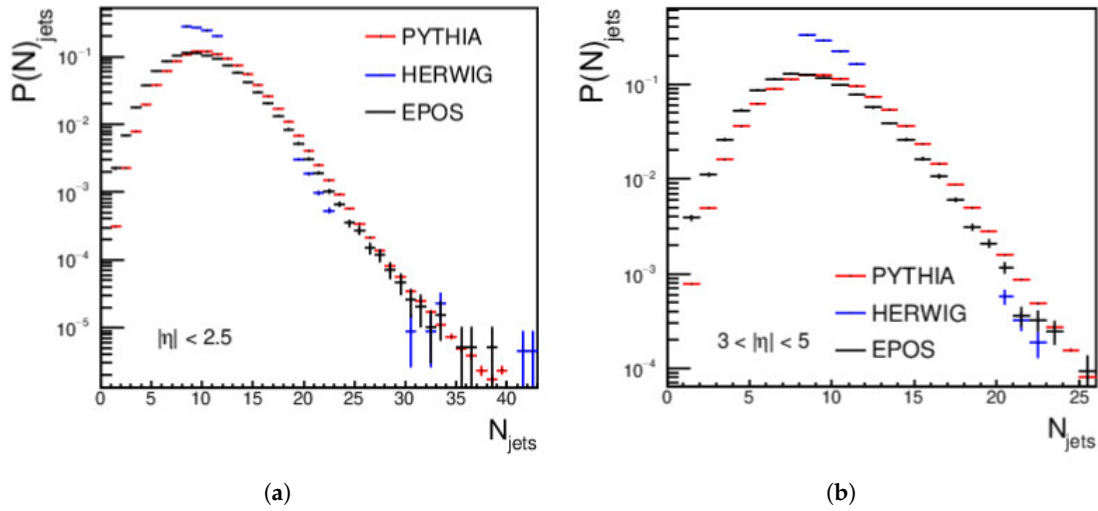


Figure 5. (a) MC comparison of jet multiplicity in the central regions at $\sqrt{s} = 20$ TeV; (b) MC comparison of jet multiplicity in the forward regions at $\sqrt{s} = 20$ TeV.

Figure 6 presents the jets’ multiplicity of the central and forward jets at energy $\sqrt{s} = 27$ TeV, with the same minimum jet $p_T > 15$ GeV/c. The central regions show a disagreement between PYTHIA, HERWIG, and EPOS-LHC, except at the peak. PYTHIA has excess data in the central and forward regions. The jet multiplicity in the central regions is larger than that in the forward regions; this is similar to the results at $\sqrt{s} = 13.6$ TeV and $\sqrt{s} = 20$ TeV. For the forward regions, an agreement between HERWIG and EPOS-LHC appears from jet multiplicities ≈ 5 –14; at the peak, PYTHIA, HERWIG, and EPOS-LHC agree with each other. Then, the spectra fall, with a clear disagreement between the three event generators.

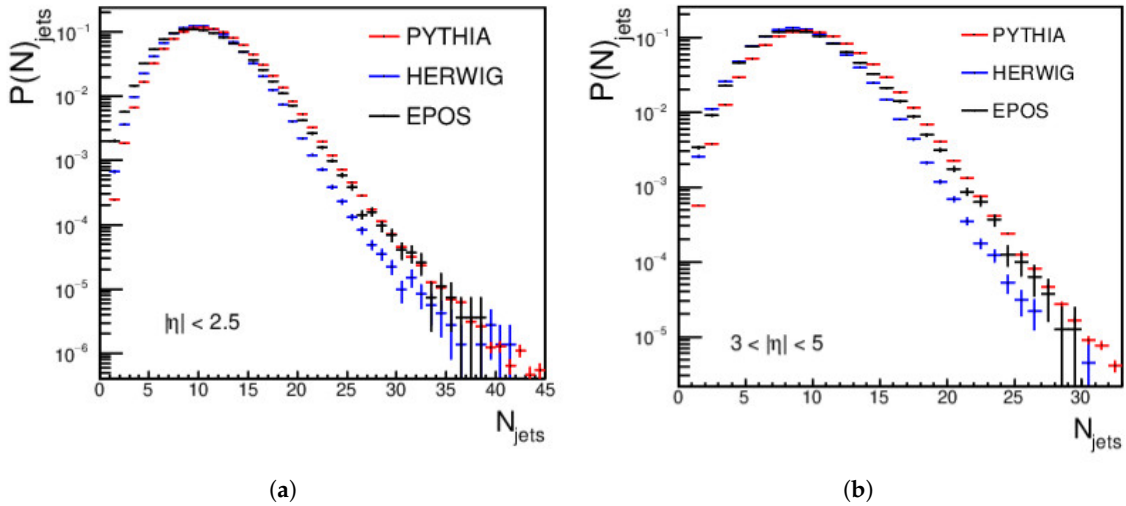


Figure 6. (a) MC comparison of jet multiplicity in the central regions at $\sqrt{s} = 27$ TeV; (b) MC comparison of jet multiplicity in the forward regions at $\sqrt{s} = 27$ TeV.

With the same cut of the minimum jet at $p_T > 15$ GeV/c, produced from the pp collisions and at energy $\sqrt{s} = 13.6$ TeV, the jet energy is presented in Figure 7. In the central and forward regions, the spectrum begins with an agreement between PYTHIA and EPOS-LHC and ends with a distinct disagreement. The results demonstrate a minor disagreement between PYTHIA, HERWIG, and EPOS-LHC, but at the far end of the spectrum, the results of three event generators differ.

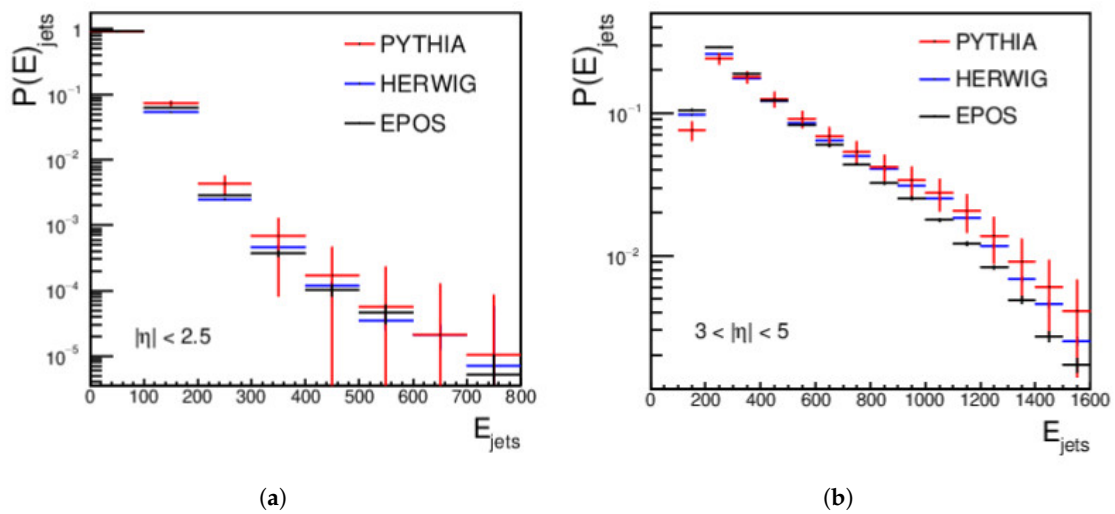


Figure 7. (a) MC comparison of central jet energy (GeV) at $\sqrt{s} = 13.6$ TeV; (b) MC comparison of forward jet energy (GeV) at $\sqrt{s} = 13.6$ TeV.

In Figure 8, the jet energy of the central and forward regions is shown at energy $\sqrt{s} = 20$ TeV, with a minimum of $p_T > 15$ GeV/c. In the central regions, the spectra start with an agreement between three event generators and fall with a small difference between them at $E \approx 200$ GeV; then, the spectra show an agreement between HERWIG and EPOS-LHC at some bins and between PYTHIA and HERWIG at some bins. In the forward and central regions, HERWIG has an excess of data. The tendency of HERWIG to produce higher-energy jets can be attributed to its softer parton shower, its matrix element corrections, and its cluster fragmentation. The energy of jets for the forward regions presents a clear agreement between the results of three event generators up to $E \approx 900$ GeV; then, a disagreement occurs.

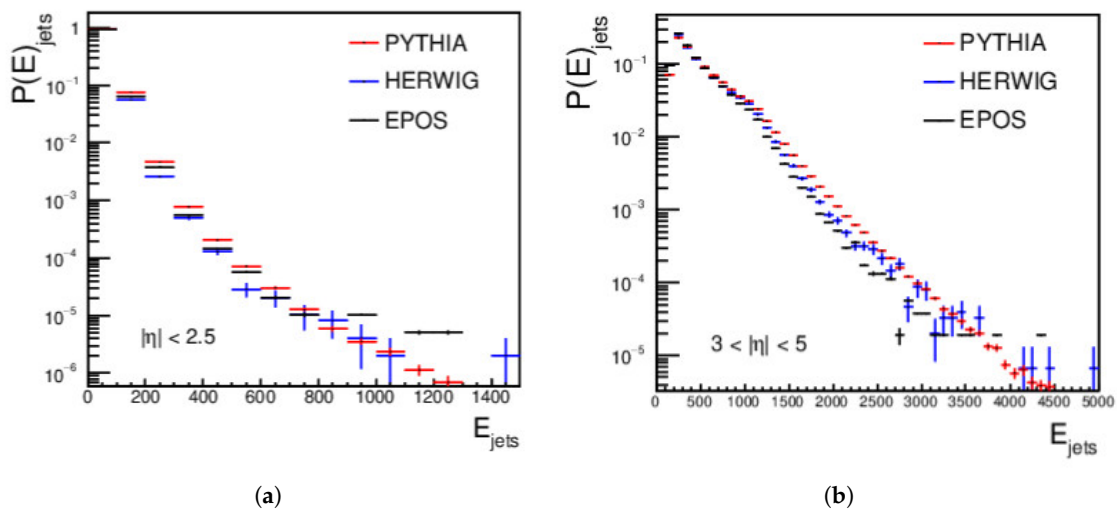


Figure 8. (a) MC comparison of central jet energy (GeV) at $\sqrt{s} = 20$ TeV; (b) MC comparison of forward jet energy (GeV) at $\sqrt{s} = 20$ TeV.

The energy of produced jets in the central and forward regions from the pp collisions with a minimum $p_T > 15$ GeV/c is shown in Figure 9 at energy $\sqrt{s} = 27$ TeV. In the central region, the distribution starts with an agreement between the three event generators and falls with a little difference between them; then, the spectra show an agreement between HERWIG and EPOS-LHC at some bins and between PYTHIA and HERWIG at some bins.

The energy spectra of the jets in the forward regions present a clear agreement between the results of the three event generators from $E \approx 400$ GeV up to $E \approx 1000$ GeV; then, a disagreement appears.

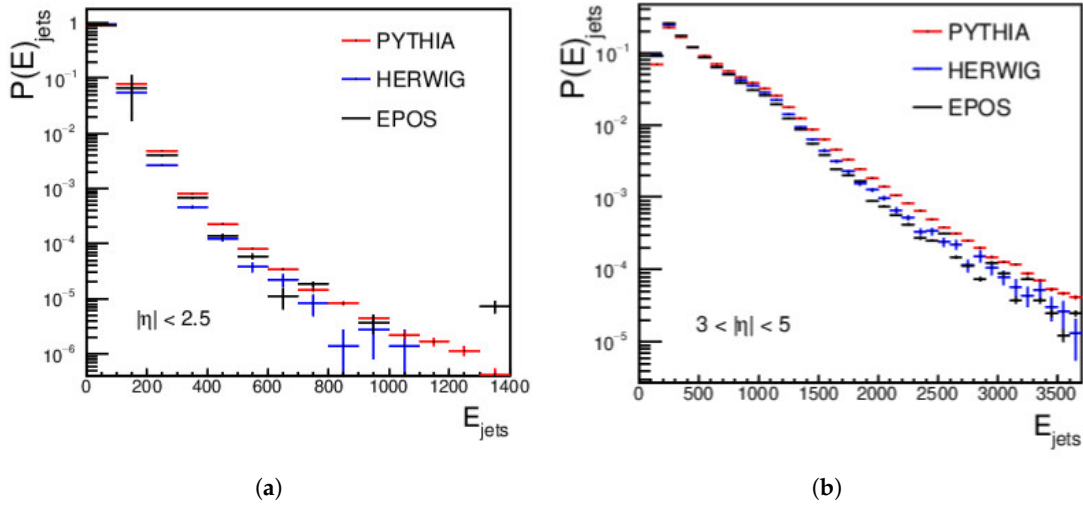


Figure 9. (a) MC comparison of central jet energy (GeV) at $\sqrt{s} = 27$ TeV; (b) MC comparison of forward jet energy (GeV) at $\sqrt{s} = 27$ TeV.

The pseudorapidity η of the forward and central jets is presented in Figure 10, with minimum $p_T > 15$ GeV/c at $\sqrt{s} = 13.6$ TeV. In the central region, the agreement between the three event generators is clear except at the peak of the spectrum. The data show good agreement between PYTHIA and HERWIG and a little disagreement with the EPOS-LHC event generator in the forward regions.

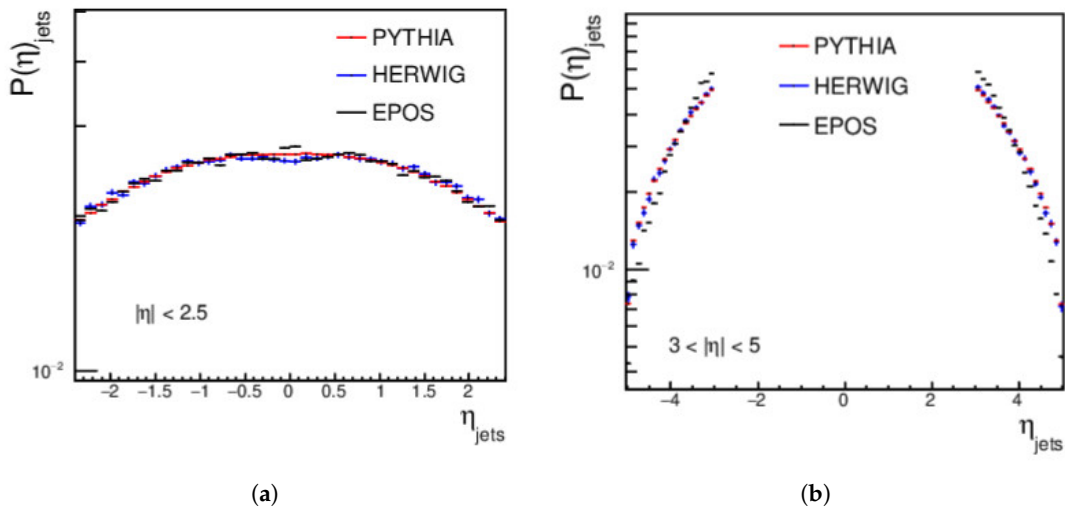


Figure 10. (a) MC comparison of η distribution in the central regions at $\sqrt{s} = 13.6$ TeV; (b) MC comparison of η distribution in the forward regions at $\sqrt{s} = 13.6$ TeV.

In Figure 11, the pseudorapidity jets produced in the forward and central jets is presented at $\sqrt{s} = 20$ TeV, with a minimum $p_T > 15$ GeV/c. For the central region, the distribution presents good agreement between three event generators, except at the middle of the spectrum, approximately in the η -range from -1 to 1 . The pseudorapidity distribution shows a good agreement between PYTHIA and HERWIG and a little disagreement with the EPOS-LHC event generator in the forward regions.

The pseudorapidity of the central and forward regions is shown in Figure 12 at energy $\sqrt{s} = 27$ TeV, with a minimum $p_T > 15$ GeV/c. In the central regions, the distribution

presents a good agreement between the three event generators. The distribution shows a little disagreement between the PYTHIA, HERWIG, and EPOS-LHC event generators in the forward regions.

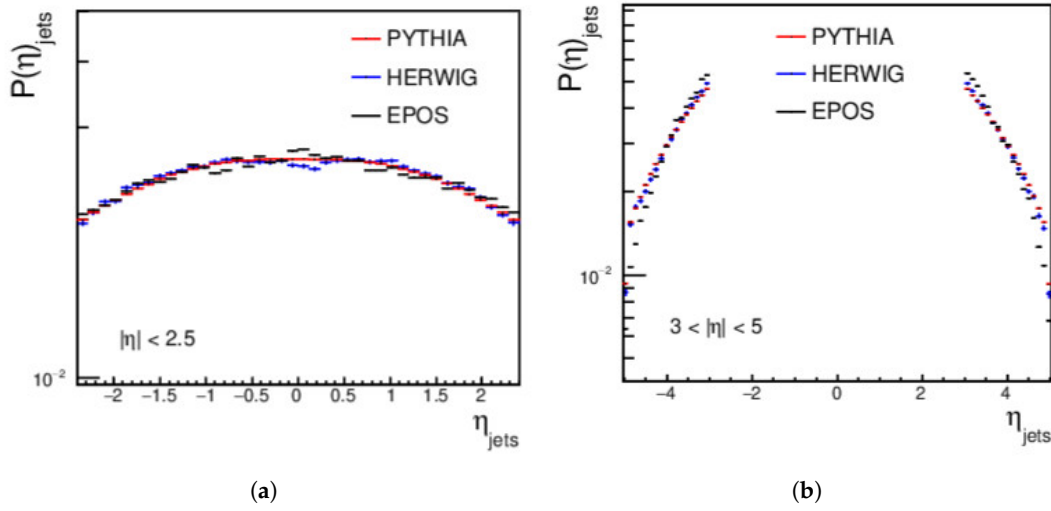


Figure 11. (a) MC comparison of η distribution in the central regions at $\sqrt{s} = 20$ TeV; (b) MC comparison of η distribution in the forward regions at $\sqrt{s} = 20$ TeV.

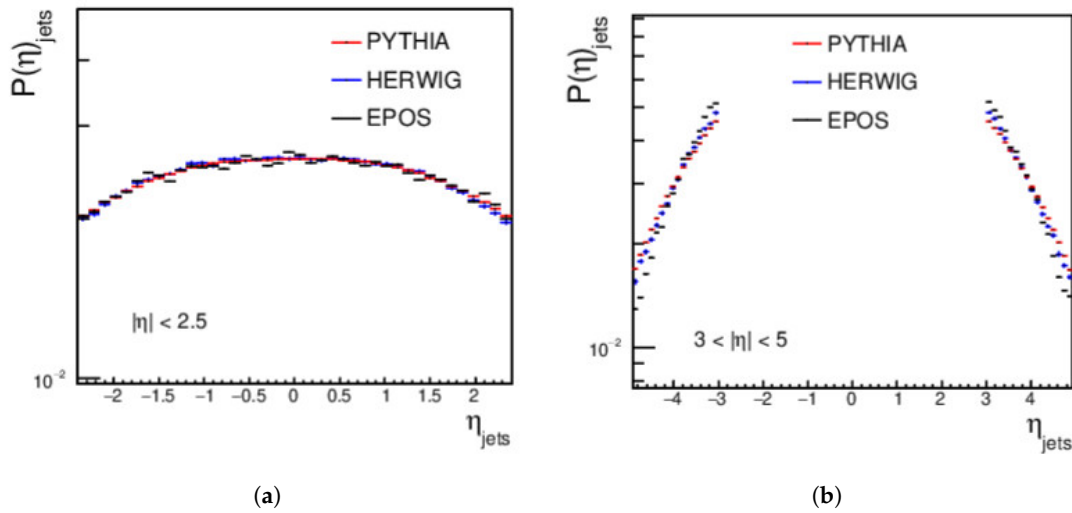


Figure 12. (a) MC comparison of η distribution in the central regions at $\sqrt{s} = 27$ TeV; (b) MC comparison of η distribution in the forward regions at $\sqrt{s} = 27$ TeV.

The azimuthal angle ϕ of the forward and central jets, with a minimum $p_T > 15$ GeV/c, is shown in Figure 13 at energy $\sqrt{s} = 13.6$ TeV. The distribution of the PYTHIA results is flat, unlike the distribution of HERWIG and EPOS-LHC in the central and forward regions; but, in the central regions, more agreement can be noted between the event generators.

The azimuthal angle ϕ of the central and forward jets is shown in Figure 14 at $\sqrt{s} = 20$ TeV with a minimum $p_T > 15$ GeV/c. The distribution of PYTHIA is more flat than those of HERWIG and EPOS-LHC in the central and forward regions; the three event generators have some agreement. For the forward regions, the HERWIG results are more flat than they are with an energy $\sqrt{s} = 13.6$ TeV.

In Figure 15, the azimuthal angle is presented with a minimum $p_T > 15$ GeV/c at an energy of $\sqrt{s} = 27$ TeV. In the central and forward regions, the PYTHIA distribution is flatter than the HERWIG and EPOS-LHC distributions. Figure 15 also indicates that there is some agreement across the event generators in the central regions. The HERWIG distribution is more flat in the forward regions than it is at energies of $\sqrt{s} = 13.6$ TeV and $\sqrt{s} = 20$ TeV.

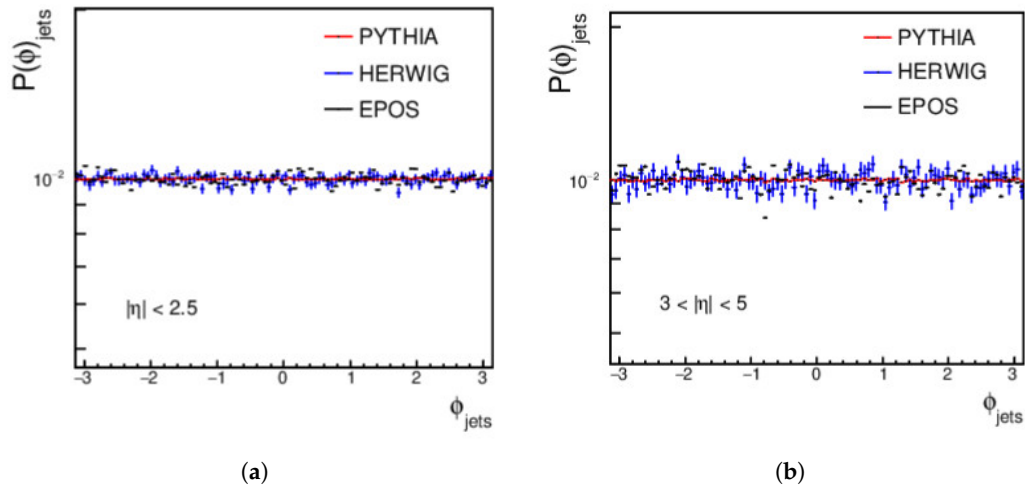


Figure 13. (a) MC comparison of ϕ (rad) distribution in the central regions at $\sqrt{s} = 13.6$ TeV; (b) MC comparison of ϕ (rad) distribution in the forward regions at $\sqrt{s} = 13.6$ TeV.

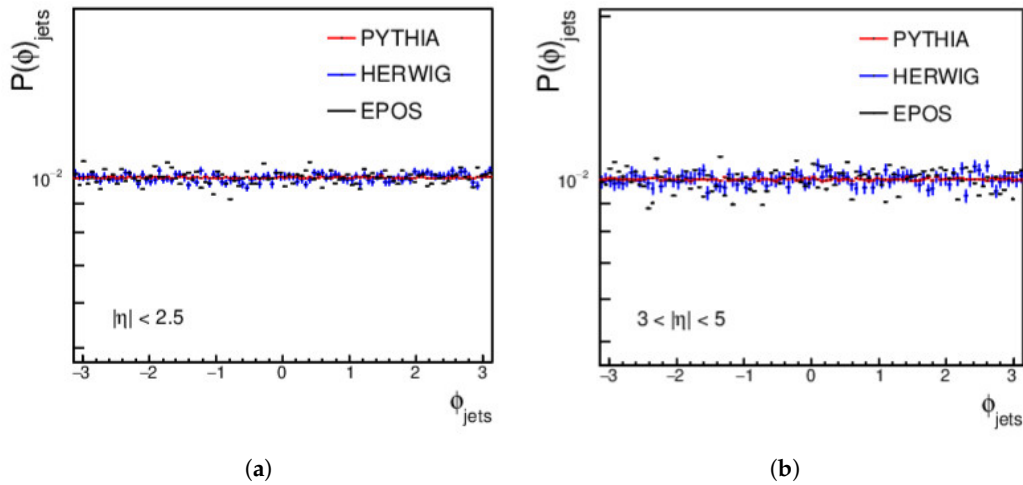


Figure 14. (a) MC comparison of ϕ (rad) distribution in the central regions at $\sqrt{s} = 20$ TeV; (b) MC comparison of ϕ (rad) distribution in the forward regions at $\sqrt{s} = 20$ TeV.

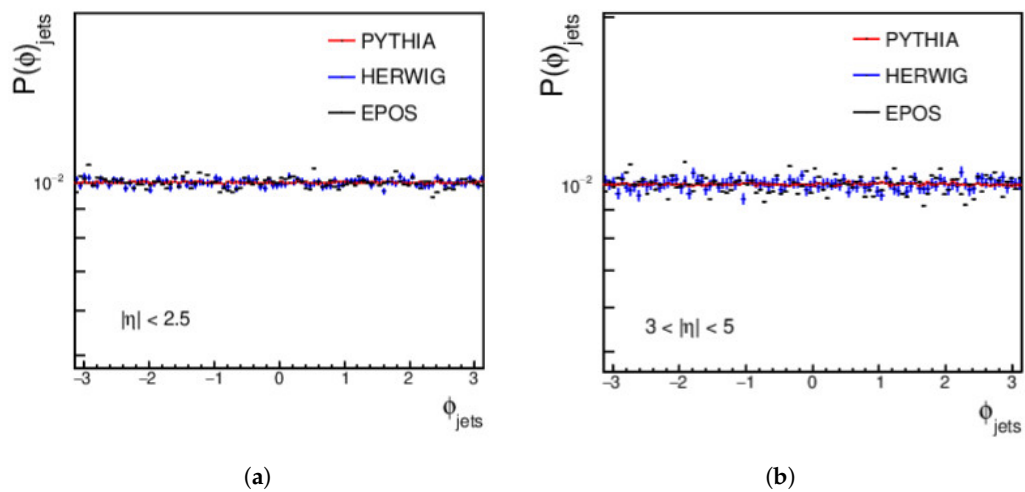


Figure 15. (a) MC comparison of ϕ (rad) distribution in the central regions at $\sqrt{s} = 27$ TeV; (b) MC comparison of ϕ (rad) distribution in the forward regions at $\sqrt{s} = 27$ TeV.

4.2. Dijets Measurements

In this section, a comparison between dijets production is presented: one is the leading central jet and the other is the sub-leading forward jet with momentum $p_T > 35$ GeV/c at different energies: $\sqrt{s} = 13.6$ TeV, $\sqrt{s} = 20$ TeV, and at $\sqrt{s} = 27$ TeV. PYTHIA, HERWIG, and EPOS-LHC event generators were used. The dijet occurrences are 2→2 parton scattering processes with a pair of jets in the final state [49]. The dijet multiplicity at the three energies starts with an agreement between PYTHIA, HERWIG, and EPOS-LHC. It is clear that the dijets multiplicity increases with increases in the energy of collision (Figure 16).

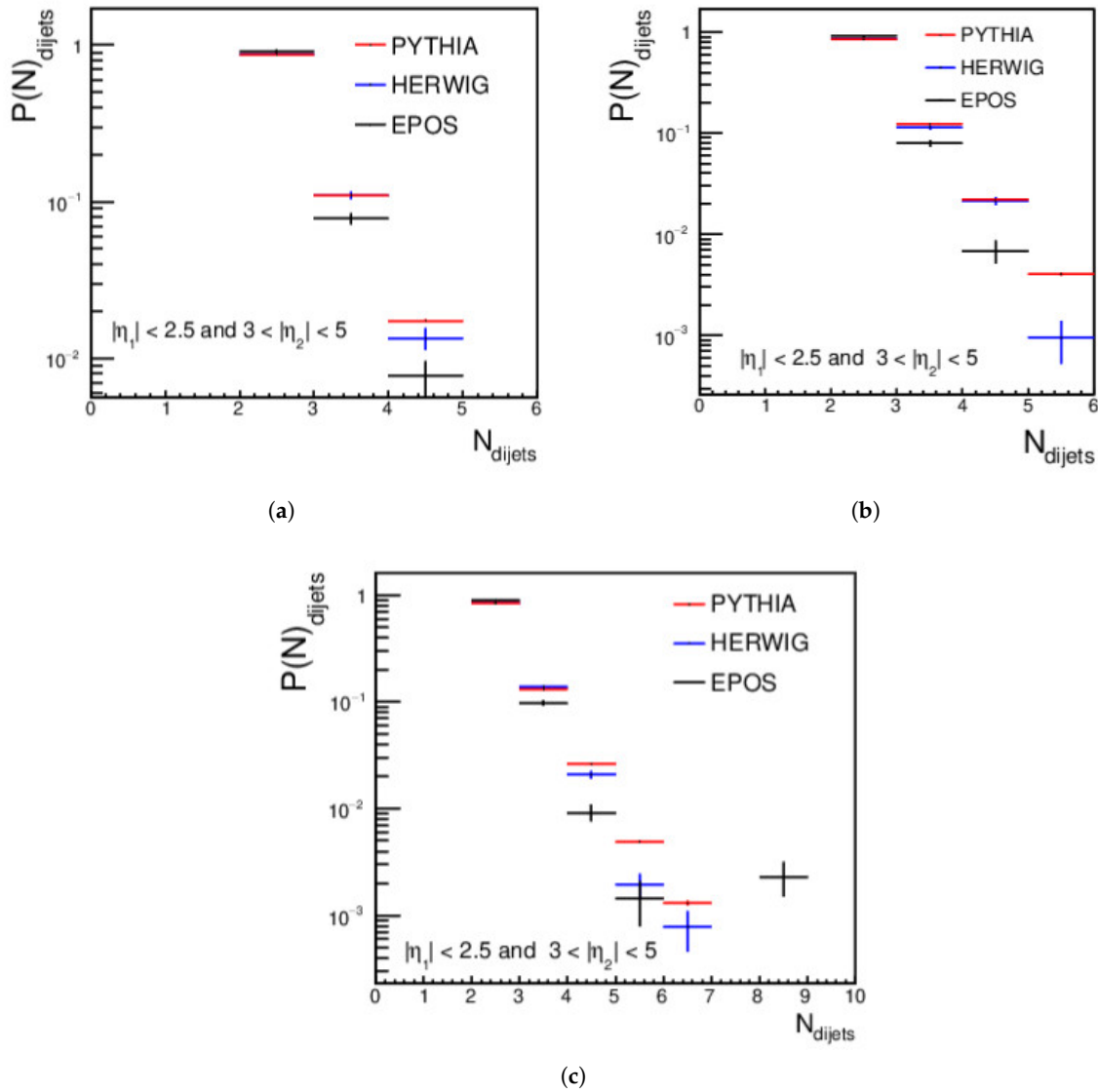


Figure 16. (a) Dijets multiplicity at energy $\sqrt{s} = 13.6$ TeV; (b) dijets multiplicity at energy $\sqrt{s} = 20$ TeV; (c) dijets multiplicity at energy $\sqrt{s} = 27$ TeV.

The $\Delta\phi$ for dijet one is leading the central jet and the other is sub-leading the forward jet, with a momentum of $p_T > 35$ GeV/c at different energies ($\sqrt{s} = 13.6$ TeV, $\sqrt{s} = 20$ TeV, and $\sqrt{s} = 27$ TeV); this was carried out using the PYTHIA, HERWIG, and EPOS-LHC event generators. See Figure 17. The results show that the distribution of PYTHIA is more well fitted than those of HERWIG and EPOS-LHC at the three energies of $\sqrt{s} = 13.6$ TeV, $\sqrt{s} = 20$ TeV, and $\sqrt{s} = 27$ TeV. Note that, as the energy of collision increases, the agreement between the results of three event generators increases. At the three energies, HERWIG has an excess of data.

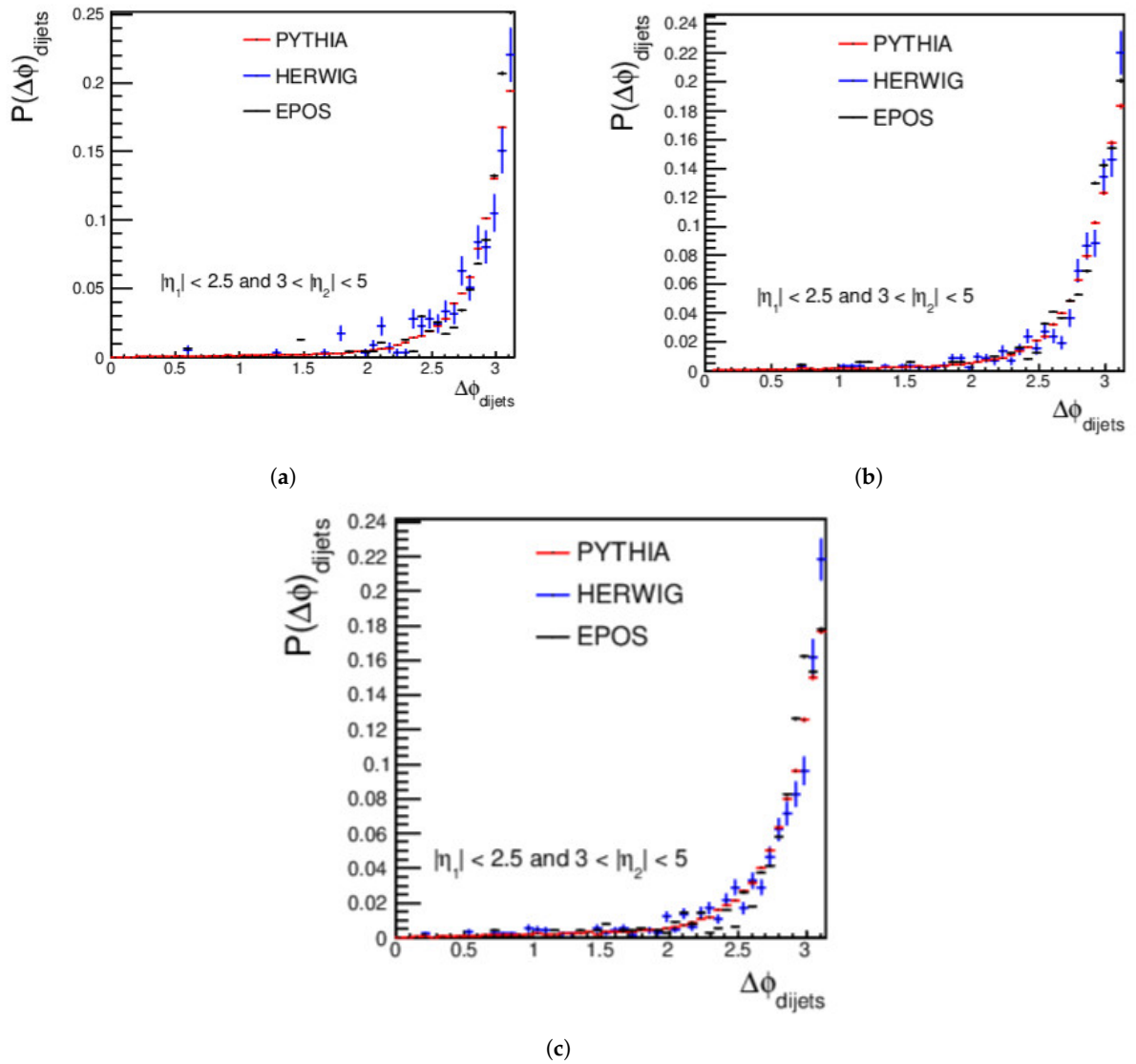


Figure 17. (a) $\Delta\phi$ (rad) distribution at energy $\sqrt{s} = 13.6$ TeV; (b) $\Delta\phi$ (rad) distribution at energy $\sqrt{s} = 20$ TeV; (c) $\Delta\phi$ (rad) distribution at energy $\sqrt{s} = 27$ TeV.

5. Conclusions

This paper presents a comprehensive study of jet production in central ($|\eta| < 2.5$) and forward ($3 < |\eta| < 5$) regions produced by pp collisions at three different energies ($\sqrt{s} = 13.6$ TeV, $\sqrt{s} = 20$ TeV, and $\sqrt{s} = 27$ TeV) using different event generators: PYTHIA, HERWIG, and EPOS-LHC. Furthermore, the measurements of dijets, where one jet serves as the leading jet and the other serves as the sub-leading jet, were investigated; one jet is in the central region and other one is in the forward region. The anti-kt ($R = 0.5$) algorithm was used for jet reconstruction within a transverse momentum range of $p_T = 15$ – 1000 GeV/c.

It is observed that the jets' and dijets' multiplicities increase as the energy of the collision increases. Furthermore, it is observed that the jet's multiplicity at central regions is larger than it is at the forward regions with the three energies; this is because the forward region encounters fewer contacts and, hence, fewer jets; the central region exhibits stronger jet generation because of the intensive parton interactions and the efficient energy transfer achieved.

HERWIG model produces higher-energy jets because of its softer parton shower, matrix element corrections, and cluster fragmentation. Furthermore, HERWIG provides

a data at high p_T , which is related to the underlying dynamics of parton interactions and hadronization.

A disagreement between different generators at some data points and an excess of data at some histograms is noticed. The possible reason for this is that each event generator depends on a different theoretical model. Although both PYHIA and HERWIG are LO MC generators, HERWIG's PS parton ordering is different from PYTHIA's. PYTHIA employs an order in the partons p_T , whereas HERWIG has adopted an angular ordering, and the EPOS-LHC event generator depends on the Gribov–Regge model.

Overall, this comparative study of the forward and central jets at future energies anticipated by the LHC offers insightful information about the characteristics of these jets and their implications for future new physics research.

Author Contributions: Methodology, M.A.M., M.A.E.-B. and E.A.T.; Software, M.A.M., S.H., A.R., M.A.E.-B. and E.A.T.; Validation, M.A.M., A.R. and M.A.E.-B.; Formal analysis, S.H.; Investigation, A.R.; Resources, A.R. and M.A.E.-B.; Data curation, S.H.; Writing—original draft, M.A.M., S.H., M.A.E.-B. and E.A.T.; Writing—review & editing, M.A.M., A.R., M.A.E.-B. and E.A.T.; Visualization, S.H.; Supervision, M.A.M., A.R. and M.A.E.-B.; Funding acquisition, A.R. All authors have read and agreed to the published version of the manuscript.

Funding: M.A. Mahmoud is supported by Science, Technology Innovation Funding Authority (STDF), Egypt under Project ID: 30163.

Institutional Review Board Statement: Not applicable.

Informed Consent Statement: Not applicable.

Data Availability Statement: No new data were created or analyzed in this study. Data sharing is not applicable to this article.

Conflicts of Interest: The authors declare no conflicts of interest.

Abbreviations

The following abbreviations are used in this manuscript:

QCD	quantum chromodynamics
MC	Monte Carlo
LHC	Large Hadron Collider
SM	standard model
BSM	beyond standard model
MPI	multiple parton interaction
ISR	initial-state radiation
FSR	final-state radiation
DM	dark matter
LO	leading order
HI	heavy ions
HEP	high-energy physics
PS	parton scattering

References

1. Frye, C.; Larkoski, A.J.; Thaler, J.; Zhou, K. Casimir meets Poisson: Improved quark/gluon discrimination with counting observables. *J. High Energy Phys.* **2017**, *2017*, 83. [[CrossRef](#)]
2. Gras, P.; Höche, S.; Kar, D.; Larkoski, A.; Lönnblad, L.; Plätzer, S.; Siódmok, A.; Skands, P.; Soyez, G.; Thaler, J. Systematics of quark/gluon tagging. *J. High Energy Phys.* **2017**, *2017*, 91. [[CrossRef](#)]
3. Gromov, N. Elementary particles in the early Universe. *J. Cosmol. Astropart. Phys.* **2016**, *2016*, 053. [[CrossRef](#)]
4. Choudhury, S. Performance of the High-Level Trigger System at CMS in LHC Run-2. *IEEE Trans. Nucl. Sci.* **2021**, *68*, 2035–2042. [[CrossRef](#)]
5. He, M.; Rapp, R. Hadronization and Charm-Hadron Ratios in Heavy-Ion Collisions. *Phys. Rev. Lett.* **2020**, *124*, 042301. [[CrossRef](#)]
6. Qu, H.; Gouskos, L. Jet tagging via particle clouds. *Phys. Rev. D* **2020**, *101*, 056019. [[CrossRef](#)]
7. Kasieczka, G.; Plehn, T.; Schell, T.; Strebler, T.; Salam, G.P. Resonance searches with an updated top tagger. *J. High Energy Phys.* **2015**, *2015*, 203. [[CrossRef](#)]

8. Kim, C. Exclusive Heavy Quark Dijet cross-section. *J. Korean Phys. Soc.* **2020**, *77*, 469–476. [[CrossRef](#)]
9. Khosa, C.K.; Marzani, S. Higgs boson tagging with the Lund jet plane. *Phys. Rev. D* **2021**, *104*, 055043. [[CrossRef](#)]
10. Sipio, R.D.; Giannelli, M.F.; Haghighat, S.K.; Palazzo, S. DijetGAN: A Generative-Adversarial Network approach for the simulation of QCD dijet events at the LHC. *J. High Energy Phys.* **2019**, *2019*, 110. [[CrossRef](#)]
11. Freytsis, M.; Volansky, T.; Walsh, J.R. Tagging partially reconstructed objects with jet substructure. *Phys. Lett. B* **2017**, 769. [[CrossRef](#)]
12. Mukhopadhyaya, B.; Samui, T.; Singh, R.K. Dynamic radius jet clustering algorithm. *J. High Energy Phys.* **2023**, *2023*, 19. [[CrossRef](#)]
13. de Lejarza, J.J.M.; Cieri, L.; Rodrigo, G. Quantum clustering and jet reconstruction at the LHC. *Phys. Rev. D* **2022**, *106*, 036021. [[CrossRef](#)]
14. Stewart, I.W.; Tackmann, F.J.; Thaler, J.; Vermilion, C.K.; Wilkason, T.F. X Cone: N-jettiness as an exclusive cone jet algorithm. *J. High Energy Phys.* **2015**, *2015*, 72. [[CrossRef](#)]
15. Marzani, S.; Soyez, G.; Spannowsky, M. *Looking Inside Jets: An Introduction to Jet Substructure and Boosted-Object Phenomenology*; Springer International Publishing: Berlin/Heidelberg, Germany, 2019. [[CrossRef](#)]
16. Boronat, M.; Fuster, J.; Garcia, I.; Roloff, P.; Simoniello, R.; Vos, M. Jet reconstruction at high-energy electron–positron colliders. *Eur. Phys. J. C* **2018**, *78*, 144. [[CrossRef](#)]
17. Moreno, E.A.; Cerri, O.; Duarte, J.M.; Newman, H.B.; Nguyen, T.Q.; Periwai, A.; Pierini, M.; Serikova, A.; Spiropulu, M.; Vlimant, J.R. JEDI-net: A jet identification algorithm based on interaction networks. *Eur. Phys. J. C* **2020**, *80*, 58. [[CrossRef](#)]
18. Tseng, J.; Evans, H. Sequential recombination algorithm for jet clustering and background subtraction. *Phys. Rev. D* **2013**, *88*, 014044. [[CrossRef](#)]
19. Sirunyan, A.; Tumasyan, A.; Adam, W.; Asilar, E.; Bergauer, T.; Brandstetter, J.; Brondolin, E.; Dragicevic, M.; Erö, J.; Flechl, M.; et al. Particle-flow reconstruction and global event description with the CMS detector. *J. Instrum.* **2017**, *12*, P10003. [[CrossRef](#)]
20. Cerro, G.; Dasmahapatra, S.; Day-Hall, H.A.; Ford, B.; Moretti, S.; Shepherd-Themistocleous, C.H. Spectral clustering for jet physics. *J. High Energy Phys.* **2022**, *2022*, 165. [[CrossRef](#)]
21. Gauld, R.; Huss, A.; Stagnitto, G. Flavor Identification of Reconstructed Hadronic Jets. Address of flavour to suit any jet. *Phys. Rev. Lett.* **2023**, *130*, 161901. [[CrossRef](#)]
22. Cukierman, A.R. *Searches for New Physics Using Jets with the ATLAS Detector*; Stanford University: Stanford, CA, USA, 2020; Volume 2020.
23. Haisch, U.; Polesello, G. Searching for dark matter in final states with two jets and missing transverse energy. *J. High Energy Phys.* **2019**, *2019*, 128. [[CrossRef](#)]
24. Sirunyan, A.M.; Tumasyan, A.; Adam, W.; Ambrogio, F.; Asilar, E.; Bergauer, T.; Brandstetter, J.; Brondolin, E.; Dragicevic, M.; Erö, J.; et al. Combined search for electroweak production of charginos and neutralinos in proton–proton collisions at $\sqrt{s} = 13$ TeV. *J. High Energy Phys.* **2018**, *2018*, 160. [[CrossRef](#)]
25. Klein, S.R.; Nystrand, J.; Seger, J.; Gorbunov, Y.; Butterworth, J. STARlight: A Monte Carlo simulation program for ultra-peripheral collisions of relativistic ions. *Comput. Phys. Commun.* **2017**, *212*, 258–268. [[CrossRef](#)]
26. Czyż, H.; Kisza, P. EKHARA 3.0: An update of the EKHARA Monte Carlo event generator. *Comput. Phys. Commun.* **2019**, *234*, 245–255. [[CrossRef](#)]
27. Baranov, S.; Martinez, A.B.; Banos, L.I.E.; Guzman, F.; Hautmann, F.; Jung, H.; Lelek, A.; Lidrych, J.; Lipatov, A.; Malyshev, M.; et al. CASCADE3 A Monte Carlo event generator based on TMDs. *Eur. Phys. J. C* **2021**, *81*, 5. [[CrossRef](#)]
28. Naseebullah; Olimov, K.K.; Khan, I.; Ali, Y.; Ajaz, M.; Ahmad, A. Analysis of production of $\Sigma(1385)_{\pm}$, $(1530)_0$ and their anti-particles in inelastic pp collisions at $\sqrt{s} = 7$ TeV. *Eur. Phys. J. Plus* **2023**, *138*, 556. [[CrossRef](#)]
29. Sjöstrand, T. The Pythia event generator: Past, present and future. *Comput. Phys. Commun.* **2020**, *246*, 106910. [[CrossRef](#)]
30. Bellm, J.; Bewick, G.; Rivasio, S.F.; Gieseke, S.; Grellscheid, D.; Kirchgaeßer, P.; Loshaj, F.; Masouminia, M.R.; Nail, G.; Papaefstathiou, A.; et al. Herwig 7.2 release note. *Eur. Phys. J. C* **2020**, *80*, 452. [[CrossRef](#)]
31. Frixione, S.; Fuks, B.; Hirschi, V.; Mawatari, K.; Shao, H.S.; Sunder, M.P.A.; Zaro, M. Automated simulations beyond the Standard Model: Supersymmetry. *J. High Energy Phys.* **2019**, *2019*, 8. [[CrossRef](#)]
32. Bothmann, E.; Chahal, G.S.; Höche, S.; Krause, J.; Krauss, F.; Kuttimalai, S.; Liebschner, S.; Napoletano, D.; Schönherr, M.; Schulz, H.; et al. Event generation with Sherpa 2.2. *SciPost Phys.* **2019**, *7*, 3. [[CrossRef](#)]
33. Ajaz, M.; Haj Ismail, A.A.K.; Muhammad, M.; Suleymanov, M.; Abdelkader, A.; Suleymanov, R. Pseudorapidity dependence of the bulk properties of hadronic medium in pp collisions at 7 TeV. *Sci. Rep.* **2022**, *12*, 8142. [[CrossRef](#)] [[PubMed](#)]
34. Tumasyan, A.; Adam, W.; Andrejkovic, J.W.; Bergauer, T.; Chatterjee, S.; Damanakis, K.; Dragicevic, M.; Escalante Del Valle, A.; Fruehwirth, R.; Jeitler, M.; et al. CMS pythia 8 colour reconnection tunes based on underlying-event data. *Eur. Phys. J. C* **2023**, *83*, 587. [[CrossRef](#)] [[PubMed](#)]
35. Brass, S.; Kilian, W.; Reuter, J. Parallel adaptive Monte Carlo integration with the event generator WHIZARD. *Eur. Phys. J. C* **2019**, *79*, 344. [[CrossRef](#)]
36. Ajaz, M.; Waqas, M.; Khan, R.; Adil Khan, M.; Li, L.L.; Alrebdi, H.I.; Abdel-Aty, A.H. Inclusive Charged-Particle Kinematic Distributions at LHC Energies: Data versus Theory. *Symmetry* **2022**, *14*, 2401. [[CrossRef](#)]

37. Bierlich, C.; Gustafson, G.; Lönnblad, L.; Tarasov, A. Effects of Overlapping Strings in pp Collisions. *J. High Energy Phys.* **2015**, *2015*, 148. [[CrossRef](#)]
38. Bellm, J.; Gieseke, S.; Grellscheid, D.; Plätzer, S.; Rauch, M.; Reuschle, C.; Richardson, P.; Schichtel, P.; Seymour, M.H.; Siódmok, A.; et al. Herwig 7.0/Herwig++ 3.0 release note. *Eur. Phys. J. C* **2016**, *76*, 196. [[CrossRef](#)]
39. Webber, B. A QCD model for jet fragmentation including soft gluon interference. *Nucl. Phys. B* **1984**, *238*, 492–528. [[CrossRef](#)]
40. Bähr, M.; Gieseke, S.; Gigg, M.A.; Grellscheid, D.; Hamilton, K.; Latunde-Dada, O.; Plätzer, S.; Richardson, P.; Seymour, M.H.; Sherstnev, A.; et al. Herwig++ physics and manual. *Eur. Phys. J. C* **2008**, *58*, 639–707. [[CrossRef](#)]
41. Ene, A.C.; Jipa, A.; Giubega, L.E. Study of Monte Carlo event generators for proton–proton collisions at LHC energies in the forward region. *Chin. Phys. C* **2019**, *43*, 083001. [[CrossRef](#)]
42. Pierog, T.; Guiot, B.; Karpenko, I.; Sophys, G.; Stefaniak, M.; Werner, K. EPOS 3 and Air Showers. *EPJ Web Conf.* **2019**, *210*, 02008. [[CrossRef](#)]
43. Drescher, H.J.; Hladik, M.; Ostapchenko, S.; Pierog, T.; Werner, K. Parton-based Gribov—Regge theory. *Phys. Rep.* **2001**, *350*, 93–289. [[CrossRef](#)]
44. Pierog, T.; Werner, K. EPOS Model and Ultra High Energy Cosmic Rays. *Nucl. Phys. B—Proc. Suppl.* **2009**, *196*, 102–105. [[CrossRef](#)]
45. Werner, K. Revealing a deep connection between factorization and saturation: New insight into modeling high-energy proton–proton and nucleus-nucleus scattering in the EPOS4 framework. *Phys. Rev. C* **2023**, *108*, 064903. [[CrossRef](#)]
46. Werner, K.; Karpenko, I.; Pierog, T.; Bleicher, M.; Mikhailov, K. Evidence for hydrodynamic evolution in proton–proton scattering at 900 GeV. *Phys. Rev. C* **2011**, *83*, 044915. [[CrossRef](#)]
47. Pierog, T.; Karpenko, I.; Katzy, J.M.; Yatsenko, E.; Werner, K. EPOS LHC: Test of collective hadronization with data measured at the CERN Large Hadron Collider. *Phys. Rev. C* **2015**, *92*, 034906. [[CrossRef](#)]
48. Bierlich, C.; Buckley, A.; Butterworth, J.; Christensen, C.H.; Corpe, L.; Grellscheid, D.; Grosse-Oetringhaus, J.F.; Gutsche, C.; Karczmarczyk, P.; Klein, J.; et al. Robust independent validation of experiment and theory: Rivet version 3. *SciPost Phys.* **2020**, *8*, 26. [[CrossRef](#)]
49. The CMS Collaboration; Sirunyan, A.M.; Tumasyan, A.; Adam, W.; Ambrogio, F.; Bergauer, T.; Dragicevic, M.; Erö, J.; Valle, A.E.D.; Flechl, M.; et al. Search for high mass dijet resonances with a new background prediction method in proton–proton collisions at $\sqrt{s} = 13$ TeV. *J. High Energy Phys.* **2020**, *2020*, 33. [[CrossRef](#)]

Disclaimer/Publisher’s Note: The statements, opinions and data contained in all publications are solely those of the individual author(s) and contributor(s) and not of MDPI and/or the editor(s). MDPI and/or the editor(s) disclaim responsibility for any injury to people or property resulting from any ideas, methods, instructions or products referred to in the content.